

Consideration of Magnetically-Induced and Conservative Electric Fields Within a Loaded Gradient Coil

Weihua Mao,¹ Blaine A. Chronik,² Rebecca E. Feldman,³ Michael B. Smith,¹ and Christopher M. Collins^{1*}

We present a method to calculate the electric (E)-fields within and surrounding a human body in a gradient coil, including E-fields induced by the changing magnetic fields and “conservative” E-fields originating with the scalar electrical potential in the coil windings. In agreement with previous numerical calculations, it is shown that magnetically-induced E-fields within the human body show no real concentration near the surface of the body, where nerve stimulation most often occurs. Both the magnetically-induced and conservative E-fields are shown to be considerably stronger just outside the human body than inside it, and under some circumstances the conservative E-fields just outside the body can be much larger than the magnetically-induced E-fields there. The order of gradient winding and the presence of conductive RF shield can greatly affect the conservative E-field distribution in these cases. Though the E-fields against the outer surface of the body are not commonly considered, understanding gradient E-fields may be important for reasons other than peripheral nerve stimulation (PNS), such as potential interaction with electrical equipment. Magn Reson Med 55:1424–1432, 2006. © 2006 Wiley-Liss, Inc.

Key words: calculations; gradient coil; electric fields; peripheral nerve stimulation; scalar potential

With the growing realization of the significance of peripheral nerve stimulation (PNS) as a limiting factor in the development and application of MRI (1–9), increasing attention has been devoted to estimating electrical (E)-fields induced by time-varying magnetic fields generated by gradient coils (10–20). Theoretically, the E-field is due not only to time-varying magnetic fields (or magnetic vector potential), but also to the electric charge distribution or scalar potential. It was previously shown that the field due to the scalar potential throughout the body is of critical importance for calculating the E-field distribution in loaded gradient coils (10,11). Another source of E-fields in gradient coils that has not yet been formally considered is the scalar potential on the windings of the coil.

To create rapid current changes in gradient coils, a very strong electromotive force is required to overcome the

inductance of the gradient winding. To create the voltage drop and drive the current, a voltage of up to thousands of volts is applied to the coil windings. The scalar potential is then a function of position along the winding, which is the source of a “conservative” E-field throughout space.

Here we present a numerical method to calculate the scalar potential along the gradient coil windings and the resulting conservative E-field within and surrounding a human body in a gradient coil. We compare these fields with those induced by the time-varying magnetic field of the same coil, and examine the effects of the order of winding the quadrants and the presence of a passive RF shield on the conservative E-field. Finally, we discuss the possibility that these fields are important for PNS.

MATERIALS AND METHODS

Gradient Coil Model and Human Body Model

A digital voxel-based model of a human male body was obtained from the products of procedures performed in previous studies (21). The model has a resolution of 5 mm and 836,518 voxels in total. Each voxel was treated as a homogeneous conductor with a uniform conductivity corresponding to the tissue at its location and the permittivity of free space.

An unshielded single-axis (*x*-axis) gradient coil was designed using constrained length/minimum inductance methods (22). The coil had a radius of 0.4 m and a length of 1.2 m. The coil inductance was calculated to be 209 μ H. The gradient efficiency was 0.046 mT/m/A. The imaging field of view (FOV, diameter of the sphere over which gradient uniformity is better than 30%) for the coil was 40 cm. The figure of merit for the coil (22) was calculated to be 0.23, which is a typical value for central imaging-region whole-body gradient coils. The coil had a total length of 80.6 m of wire wound into four quadrants with 10 loops each. The wire was divided into 3652 segments, and each segment could be treated as a short straight current element. Figure 1 gives a side view of the gradient coil quadrants, which are identified as A, B, C, and D for reference in this work.

Four different RF shields were modeled, including a long continuous cylinder, a short continuous cylinder, a long cylinder with eight complete longitudinal slits to inhibit formation of eddy currents, and a short cylinder with eight such slits. All of the RF shields had a radius of 0.35 m. The longer shield had a length equal to that of the gradient coil (1.2 m), while the shorter shield had a length equal to half that of the gradient coil (60 cm).

The quasistatic approximation was applied in these calculations. This is equivalent to ignoring the effects of 1) wavelength, 2) skin depth, and 3) tissue permittivity. Al-

¹Department of Radiology, Pennsylvania State University College of Medicine, Hershey, Pennsylvania, USA.

²Department of Physics and Astronomy, University of Western Ontario, London, Ontario, Canada.

³Department of Medical Biophysics, University of Western Ontario, London, Ontario, Canada.

Grant sponsor: NIH; Grant number: R21 EB001519.

*Correspondence to: Christopher M. Collins, Center for NMR Research, NMR/MRI Building, Department of Radiology H066, Pennsylvania State University College of Medicine, 500 University Drive, Hershey, PA 17033. E-mail: cmcollins@psu.edu

Received 2 May 2005; revised 12 December 2005; accepted 13 February 2006.

DOI 10.1002/mrm.20897

Published online 5 May 2006 in Wiley InterScience (www.interscience.wiley.com).

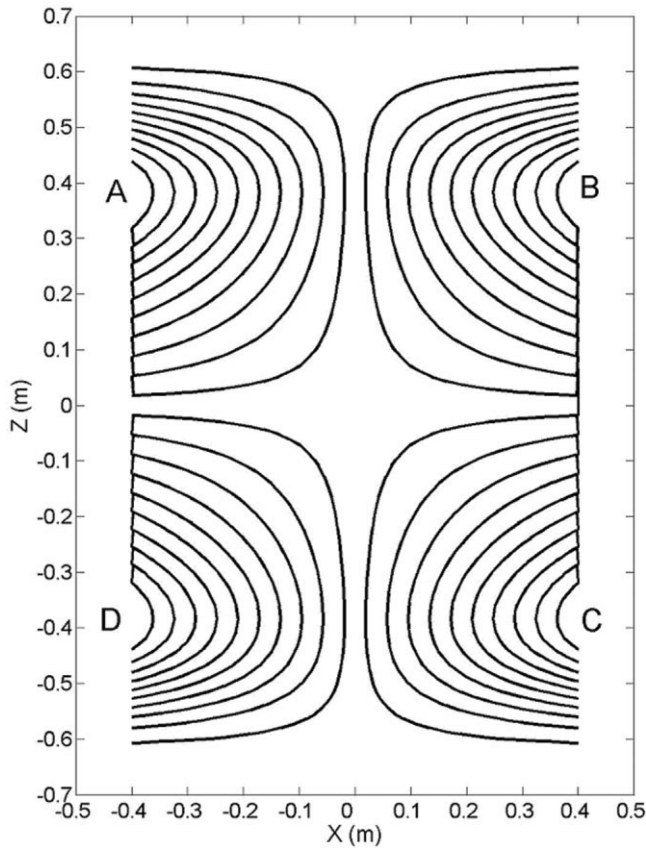


FIG. 1. The x-axis gradient winding pattern. The different winding quadrants are labeled **A-D**.

though the last element of the quasistatic approximation is the least accurate for this application, it has been shown that it is sufficiently accurate for these calculations (15,16).

Calculation of Source Magnetic Field

There are two major primary sources of E-fields in gradient coils. The first, the time-varying vector potential (**A**) or magnetic field ($\mathbf{B} = \nabla \times \mathbf{A}$), is the one most often considered in calculations regarding PNS. Here we will refer to the E-field induced directly by the time-varying **A** as \mathbf{E}_A :

$$\mathbf{E}_A = -\frac{\partial \mathbf{A}}{\partial t} \quad [1]$$

Here **A** was calculated throughout space directly from gradient coil current (*I*) as

$$\mathbf{A}(\mathbf{r}) = \frac{\mu_0}{4\pi} \sum_N \frac{I_n \mathbf{l}_n}{|\mathbf{r} - \mathbf{r}'_n|} \quad [2]$$

where **r** is a vector indicating spatial location, μ_0 is the magnetic permeability of free space, the summation is performed over all *N* segments of the coil, \mathbf{l}_n is a vector indicating the length and orientation of the *n*th segment, and \mathbf{r}'_n is a vector indicating the position of the *n*th segment.

Calculation of the Source Scalar Potential

The second primary source of E-fields within gradient coils is the voltage distribution along the wire windings required to drive the necessarily large currents in the presence of the large coil inductance. The total inductance *L* of each segment *m* was determined after the Neumann formula was used to calculate the inductance between it and all other segments *n*:

$$L_m = \frac{\mu_0}{4\pi} \sum_{\substack{n=1:N \\ n \neq m}} \frac{\mathbf{l}_m \cdot \mathbf{l}_n}{r_{mn}} \quad [3]$$

where **l** is a vector containing information on segment length and current direction for elements *m* and *n*, and r_{mn} is the distance between the segments. Here it is assumed that all elements carry unit current (1A). The scalar potential along the wire was calculated so as to produce the voltage drops necessary to drive the desired current in the presence of the resulting inductance pattern and ignoring the resistance of the wire:

$$d\phi_m = L_m \frac{dI}{dt} \quad [4]$$

where $d\phi_m$ is the potential drop across segment *m*, and dI/dt is the desired rate of change in the current. During gradient switching the resistance of the wire is negligible compared to the inductive impedance. One can calculate the relative distribution of ϕ throughout the wire, ϕ_w , after defining the location of the driving voltage and insisting that ϕ_w be continuous elsewhere along the wire. The resulting ϕ_w is then held constant as the scalar potential within the coil volume is calculated using the methods described below.

Scalar Potential in Passive Conductors

Both of the primary sources of E-fields induce currents and/or redistribution of charges in passive conductors, including the human body. These redistributed charges can then be seen as a secondary source of E-fields. The electric charge density and scalar potential in a conductor are restricted by two conditions. First of all, the system is treated as quasistatic, or the current is continuous everywhere in the conductor as expressed in the continuity equation:

$$\nabla \cdot \mathbf{J} = 0 \quad [5]$$

According to Ohm's law, current density **J** is determined by its conductivity σ and corresponding E-field:

$$\mathbf{J}^{i,j,k} = \sigma^{i,j,k} \mathbf{E}^{i,j,k} \quad [6]$$

where *i,j,k* indicate grid positions and in general

$$\mathbf{E} = -\frac{\partial \mathbf{A}}{\partial t} - \nabla \phi = \mathbf{E}_A - \nabla \phi \quad [7]$$

To obtain high accuracy, the location of E-field is shifted by half a cell from that of scalar potential in a cubic grid with a cell size of Δ in discretization of Eq. [7]. Because the scalar potential of the cube is approximately equal to the scalar potential in the center of the cell, the calculated E-field should be close to the E-field on the boundary between cubes, or at the face center of each cube.

Consequently, Eq. [5] is discretized to

$$J_x^{i-\frac{1}{2},k} - J_x^{i+\frac{1}{2},k} + J_y^{i,j-\frac{1}{2},k} - J_y^{i,j+\frac{1}{2},k} + J_z^{i,j,k-\frac{1}{2}} - J_z^{i,j,k+\frac{1}{2}} = 0 \quad [8]$$

The x components of current density are calculated as

$$\begin{aligned} \phi_{n+1}^{i,j,k} = \Delta \frac{\sigma^{i-1,j,k} E_{Ax}^{i-\frac{1}{2},k} - \sigma^{i+1,j,k} E_{Ax}^{i+\frac{1}{2},k} + \sigma^{i,j-1,k} E_{Ay}^{i,j-\frac{1}{2},k} - \sigma^{i,j+1,k} E_{Ay}^{i,j+\frac{1}{2},k} + \sigma^{i,j,k-1} E_{Az}^{i,j,k-\frac{1}{2}} - \sigma^{i,j,k+1} E_{Az}^{i,j,k+\frac{1}{2}}}{\sigma^{i-1,j,k} + \sigma^{i+1,j,k} + \sigma^{i,j-1,k} + \sigma^{i,j+1,k} + \sigma^{i,j,k-1} + \sigma^{i,j,k+1}} \\ + \frac{\sigma^{i-1,j,k} \phi_n^{i-1,j,k} + \sigma^{i+1,j,k} \phi_n^{i+1,j,k} + \sigma^{i,j-1,k} \phi_n^{i,j-1,k} + \sigma^{i,j+1,k} \phi_n^{i,j+1,k} + \sigma^{i,j,k-1} \phi_n^{i,j,k-1} + \sigma^{i,j,k+1} \phi_n^{i,j,k+1}}{\sigma^{i-1,j,k} + \sigma^{i+1,j,k} + \sigma^{i,j-1,k} + \sigma^{i,j+1,k} + \sigma^{i,j,k-1} + \sigma^{i,j,k+1}} \quad [11] \end{aligned}$$

which can be shown to be equivalent to previously reported formulations (13).

Equation [11] indicates that the scalar potential at one location within the conductor depends on the scalar potential distribution and source magnetic field at neighboring locations, unless that neighboring location is in a material with no conductivity. It is interesting that the scalar potential at any location outside the conductor does not contribute to the scalar potential distribution within the conductor. This implies that the conductor's internal scalar potential distribution is independent of external ϕ and E_A . If the conductor scalar potential distribution is floating and is changed uniformly by some value, it still satisfies Eq. [11]. This can be understood by considering the accumulation of charges on the outer surface of the conductor, which serve to shield the interior of the conductor from external fields. In fact, the external scalar potential distribution will affect the electrical charge distribution on the conductor surface significantly.

To determine the scalar potential level of the passive conductor relative to external values, a second restriction that the human body should have zero net charge is imposed. This is equivalent to the situation for a human subject undergoing MRI, during which the subject is usually not grounded. The scalar potential satisfies the Poisson equation:

$$\nabla^2 \phi = -\frac{\rho}{\epsilon} \quad [12]$$

where ρ is the charge density, and ϵ is the electric permittivity. This can be discretized as

$$-\frac{\rho^{i,j,k}}{\epsilon} = \nabla^2 \phi^{i,j,k} \approx (\phi^{i-1,j,k} + \phi^{i+1,j,k} + \phi^{i,j-1,k} + \phi^{i,j+1,k} + \phi^{i,j,k-1} + \phi^{i,j,k+1} - 6\phi^{i,j,k})/\Delta^2 \quad [13]$$

$$J_x^{i+\frac{1}{2},k} = \sigma^{i+1,j,k} E_x^{i+\frac{1}{2},k} = \sigma^{i+1,j,k} \left(E_{Ax}^{i+\frac{1}{2},k} - \frac{\phi^{i+1,j,k} - \phi^{i,j,k}}{\Delta} \right) \quad [9]$$

and

$$J_x^{i-\frac{1}{2},k} = \sigma^{i-1,j,k} E_x^{i-\frac{1}{2},k} = \sigma^{i-1,j,k} \left(E_{Ax}^{i-\frac{1}{2},k} - \frac{\phi^{i,j,k} - \phi^{i-1,j,k}}{\Delta} \right) \quad [10]$$

and other components are calculated similarly. E_{Ax} , E_{Ay} , and E_{Az} are three orthogonal components of E_A in Cartesian coordinates.

Replacing current density components, the scalar potential can be calculated iteratively as

in the cubic grid with a cell size of Δ , so that the total net charge is calculated as

$$Q = \iiint_{\text{conductor}} \rho d^3r \approx \sum_{i,j,k} (\rho^{i,j,k} \Delta^3) \approx -\epsilon \Delta \sum_{i,j,k} (\phi^{i-1,j,k} + \phi^{i+1,j,k} + \phi^{i,j-1,k} + \phi^{i,j+1,k} + \phi^{i,j,k-1} + \phi^{i,j,k+1} - 6\phi^{i,j,k}) \quad [14]$$

Zero-net-charge ($Q = 0$) is enforced by iteratively shifting the conductor scalar potential proportionally to the total net charge calculated in the previous step. This step is not performed for other passive conductors (i.e., RF shield or RF shield segments) because they are assumed to be grounded.

Scalar Potential in Free Space

In free space where $\rho = 0$, Eq. [12] becomes a Laplace equation and can be calculated by an iterative relaxation method in a cubic grid. This method iteratively uses the simple average of the scalar potentials of the six nearest neighbors at each point in space, while holding ϕ at the source (within the wires) constant:

$$\phi_n^{i,j,k} = (\phi_n^{i-1,j,k} + \phi_n^{i+1,j,k} + \phi_n^{i,j-1,k} + \phi_n^{i,j+1,k} + \phi_n^{i,j,k-1} + \phi_n^{i,j,k+1}) \div 6 \quad [15]$$

Here the superscript indicates the grid location, and the subscript indicates the iteration order.

Calculation Order

Generally, four steps are needed to calculate the complete scalar potential distribution:

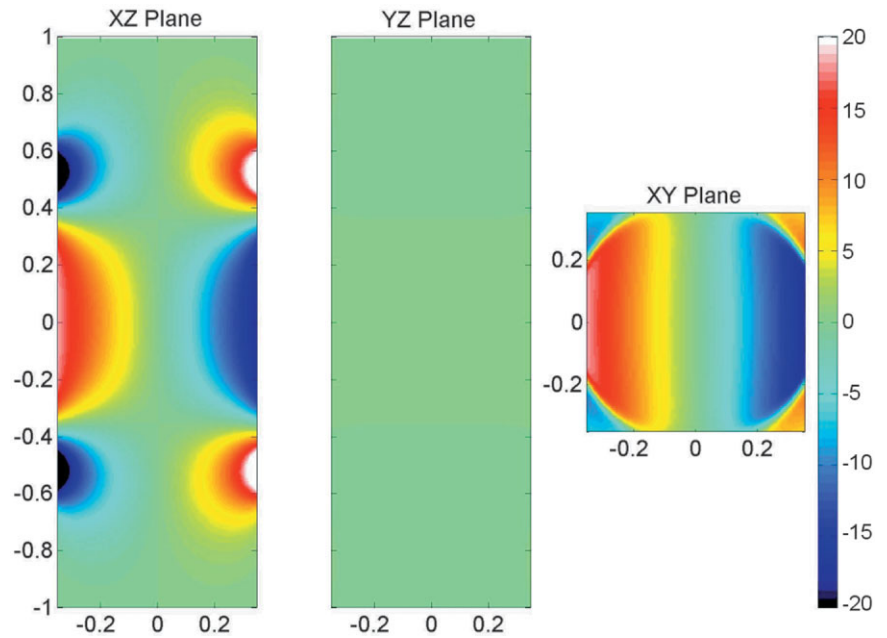


FIG. 2. B_z distribution on orthogonal planes through the center of the x -axis gradient coil. The scale is in Tesla/MA.

1. Calculate the \mathbf{A} and \mathbf{E}_A distributions directly from the gradient coil current (Eqs. [1] and [2]). \mathbf{E}_A will be used as constant field in later calculations.

2. Calculate the inductance of each gradient coil wire filament directly from the gradient coil current (Eq. [3]) and determine the scalar potential distribution along the gradient coil wire ϕ_w , which will also be held constant throughout the remaining steps (Eqs. [3] and [4]).

3. Iteratively calculate the scalar potential distribution within the conductors from \mathbf{E}_A (sample and RF shield) independently (Eq. [11]).

4. Iteratively calculate the scalar potential distribution in surrounding free space (Eq. 15) and shift the conductor scalar potential distribution in the sample (assume the shield is grounded) to maintain zero-net-charge (Eq. [14]). Note that at this stage the scalar potential in free space will be affected not only by ϕ_w , but also by ϕ in all conductors.

Typically, the conductor scalar potential distribution converges in less than 100000 iterations. Once the scalar potential distribution is known, the E-field is calculated by Eq. [7].

The magnetic field strength throughout the coil was calculated using the Biot-Savart law and the same discretized wire pattern used above. The scalar potential, vector potential, and total E-fields are proportional to the slew rate. All calculations are for a slew rate of 46 T/m/s, resulting from a current change of 1 MA/s in the complete coil. This is equivalent to driving the coil with 209 V. Calculations were performed on an $181 \times 181 \times 501$ grid with a 5-mm resolution. Calculations were performed for cases considering only \mathbf{E}_A as a source, and considering both ϕ_w and \mathbf{E}_A with and without gradient shield windings, in the presence of grounded RF shields of different geometries, and different orders of gradient coil winding. In all cases the human body model was positioned such that its center was aligned with the center of the coil. The outer boundary condition of $\phi = 0$ was applied. This is a reasonable first approximation because the gradient coils and human body are surrounded by a grounded metallic magnet casing.

RESULTS

Figure 2 shows the distribution of \mathbf{B}_z for the coil model as calculated with the Biot-Savart law. The gradient at the center of the coil is primarily in the left-right (x) direction on the xz (coronal) plane, as expected for an x -axis gradient coil. Figure 3 illustrates magnetically-induced E-field \mathbf{E}_A in the empty and loaded gradient coils. The E-field strength reaches a few V/m in the imaging region with a current increase rate of 1 MA/s. This corresponds to the calculations performed in most previous studies, ignoring the scalar potential in the coil windings and the resulting conservative E-fields. The total E-field throughout the empty and loaded coils, including the effects of the scalar potential on the wires ϕ_w , is shown in Fig. 4. The color scale is very different because the field maxima are approximately 100 times larger than when the effects of ϕ_w are not considered. In the loaded case the strongest E-field exists around the right upper arm of the model (close to quadrant A). This is because in this configuration the driving voltage is high at the beginning of windings for quadrant A, and is zero at the end of windings for quadrant D. Figure 5 presents the effects of changing the quadrant order on the E-field. The effects of different grounded RF shields are compared in Fig. 6.

DISCUSSION

Comparative Nature of Magnetically-Induced and Conservative E-Fields

In the simple case considered in these calculations, it is shown that both the vector potential \mathbf{A} produced by the currents in the gradient coil, and the scalar potential along its wire, ϕ_w , can produce E-fields throughout the volume of the gradient coil. In the empty coil the conservative fields (whose primary source is in ϕ_w) can be much stronger than the magnetically-induced E-fields (whose primary source is in $d\mathbf{A}/dt$). In the presence of a conductive sample, such as the human body, both the conservative and magnetically-in-

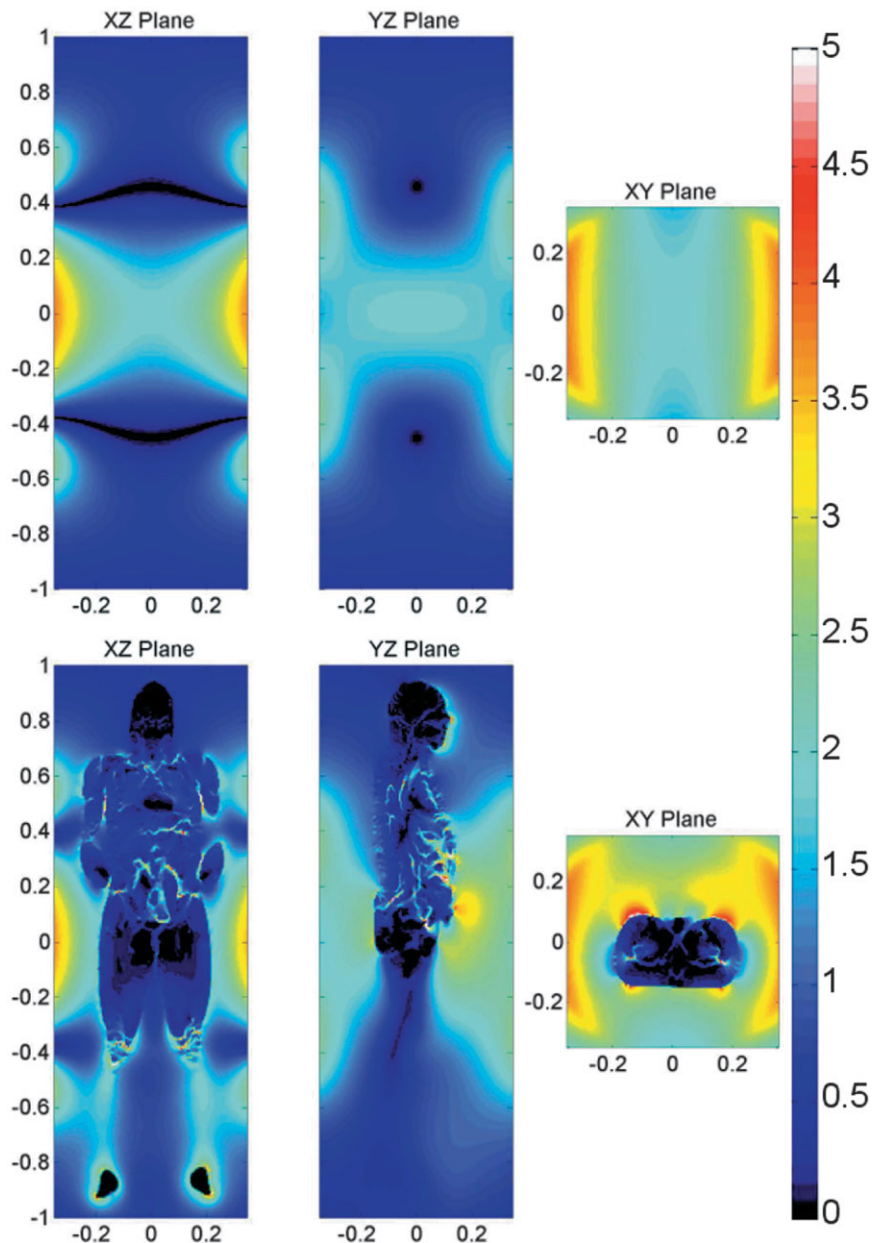


FIG. 3. Magnetically-induced E-field in the empty gradient coil (top) and the loaded gradient coil (bottom) due to the time-varying magnetic field. The dI/dt through the coil is 1 MA/s. The scale is in V/m.

duced E-fields induce electric currents that result partially in an accumulation of charges at boundaries between materials of differing conductivity and thus alters the scalar potential distribution and E-field distribution throughout the coil volume. These currents can be thought of as two different types: brief noncirculating currents that result in accumulation of charge at an outer boundary of the conductor that opposes and quickly negates the E-field inducing the current, and longer-lived circulating currents related to E-fields with non-zero curl components.

Applied E-fields that have a nonzero curl component can induce currents that circulate within the body without being terminated by a boundary with air. Magnetically-induced E-fields can have a nonzero curl component in the body, whereas conservative E-fields, which are induced by ϕ_w , can not because these fields are the result of $\nabla \phi$. Thus, a portion of the E-fields induced by $d\mathbf{A}/dt$ can penetrate

the body, while those induced by ϕ_w and another, noncirculating portion produced by $d\mathbf{A}/dt$ will be shielded from the body by charges accumulating at the surface. As a result, while the E-fields surrounding the body generally must be calculated considering the sources in $d\mathbf{A}/dt$, ϕ_w , and ϕ in the passive conductors and body, the E-fields within the body generally can be calculated without considering ϕ_w or ϕ in conductors outside the body.

In the calculations presented here (Fig. 3) and elsewhere (13,17–20), the magnetically-induced E-fields and currents within the body are very heterogeneous, and discontinuities related to internal anatomy are clearly apparent. Electrical currents flowing across boundaries between tissues with dissimilar conductivities result in some charge accumulation at these boundaries, such that current and E-field distributions are dependent on internal anatomy.

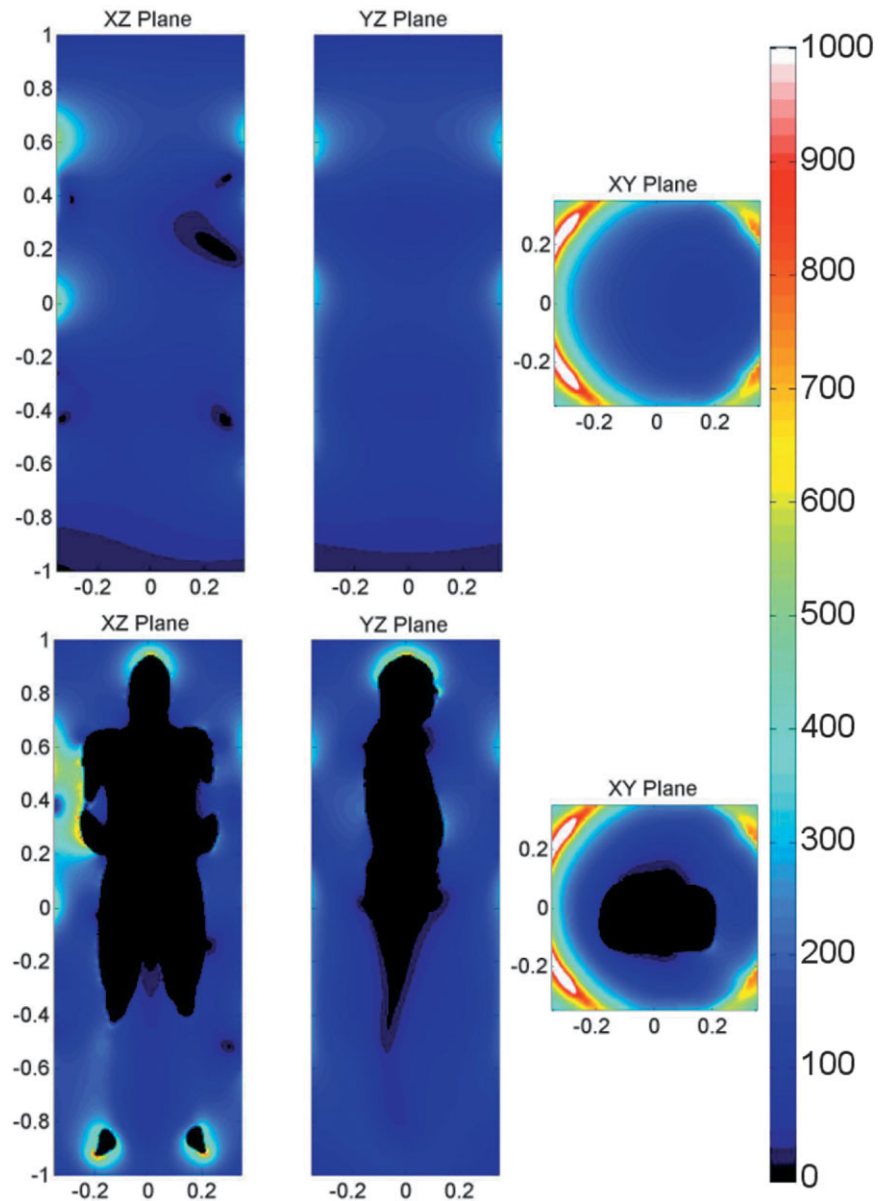


FIG. 4. Total E-field distribution (magnetically-induced plus conservative E-fields) within the empty (top) and loaded (bottom) x-axis gradient coil. The coil is being driven at 1 MA/s and the E-fields are shown in units of V/m. As expected, the conservative contributions do not penetrate the body as do the magnetically-induced contributions.

In Fig. 4 there are notable E-fields near the head and feet of the human subject, though these parts of the body are relatively far away from the coil. This is because in these simulations the scalar potential of the entire body is allowed to drift in the positive direction relative to ground (in the direction of ϕ_w), and a gradient in scalar potential toward the zero-potential boundary, or grounded metallic magnet casing, results in this E-field. The magnitude of this field in these regions is reduced with the presence of an RF shield (Fig. 6) because the coupling between the coil and the body is reduced and the scalar potential of the body remains closer to ground potential (its assumed initial starting point).

Figure 5 compares the E-fields resulting from different quadrant driving orders. The scalar potential distribution was reorganized because it highly depends on the winding order, while the winding order has no effect on magnetic field or vector potential.

Figure 6 illustrates that a long continuous RF shield can screen most of the conservative E-field. This acts as a

Faraday cage to shield out the effects of the conservative E-field. A short continuous RF shield can partly affect the conservative E-field distribution within the length of the shield, but the effect is not straightforward because the shield is grounded, and the potential of the body will become nonzero due to coupling to the gradient coil. Calculations for shields segmented with longitudinal slits showed that they largely screen the conservative E-fields, although ideally they would have no effect on \mathbf{B} or \mathbf{A} . Thus, in these calculations, it appears that the strength of the conservative E-fields can be reduced below those of the magnetically-induced fields if a long RF shield is present. Often such a shield is present between the body gradient and the subject because of the presence of a body volume RF coil; however, the length of such a shield is not standard and can make a significant difference (Fig. 6). In head and limb gradient coils the presence of such a shield or effective Faraday cage more likely depends on the RF coil chosen for a given experiment.

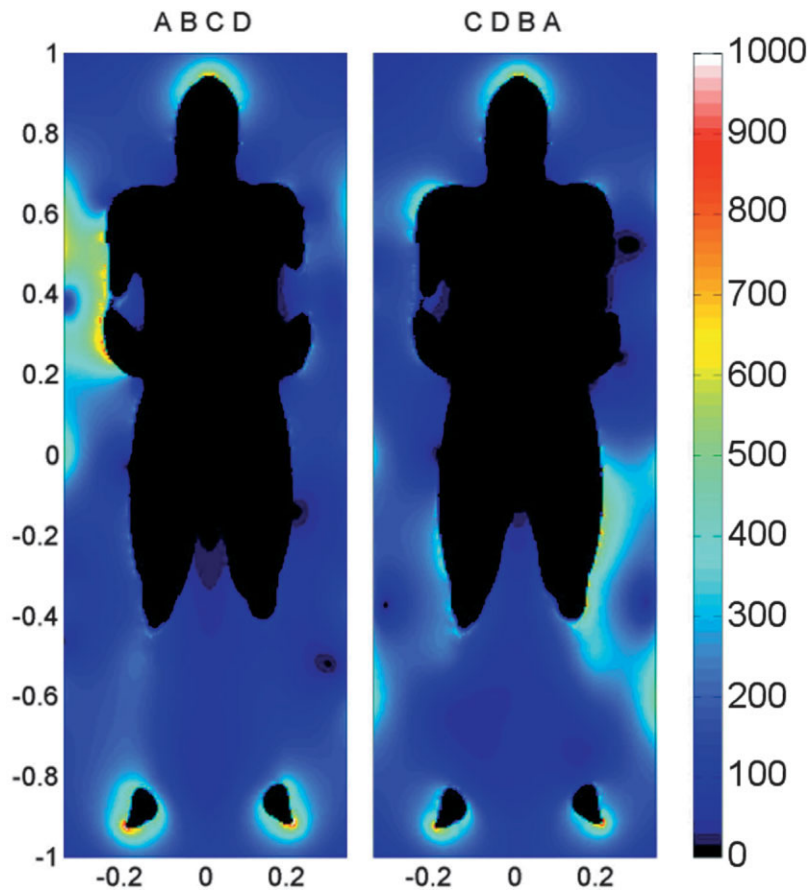


FIG. 5. Total E-field distribution on the xz plane with different quadrant driving orders, as indicated above each plot. The driving voltage is high (positive) at the beginning of the winding, and zero at the end. The quadrants are as in Fig. 1 (quadrant **A**: upper left; quadrant **B**: upper right; quadrant **C**: lower right; quadrant **D**: lower left; where right and left are defined from the reader's perspective). The scale is in V/m.

Limitations of the Presented Conservative E-Field Calculations

Because of the simple coil geometry considered, the results of the calculations of conservative E-fields presented here have very limited applicability to real gradient coils. As shown in Fig. 6, the presence of a grounded passive RF shield can effectively shield the imaging region from the

conservative E-fields, provided that the shield is long enough. Besides an RF shield, other conductors between a gradient coil and the sample will effectively shield the sample from the conservative E-fields. In a realistic imaging environment this will ensure that only the conservative E-fields from the innermost gradient windings will have significant magnitude in the imaging region, and

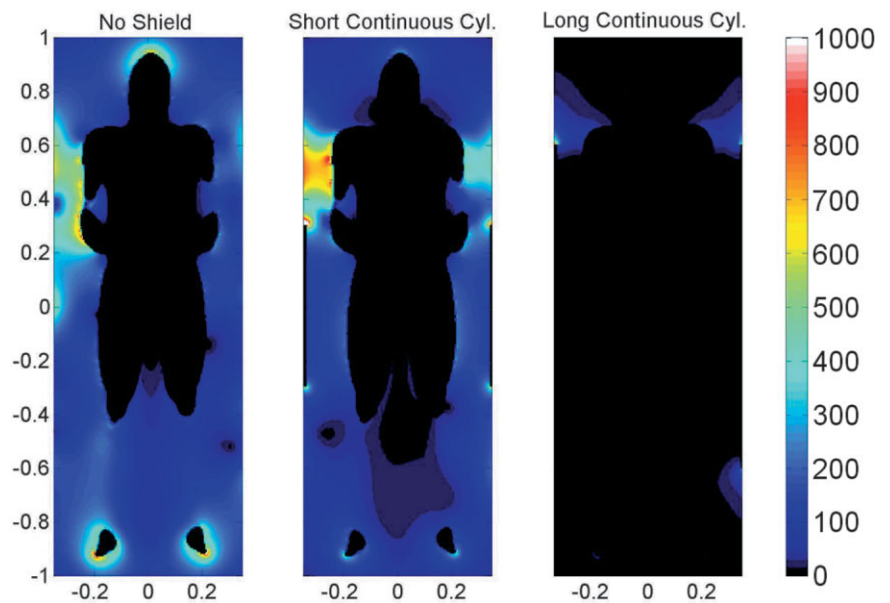


FIG. 6. Total E-field distribution on the xz plane with different RF shields. The scale is in V/m.

indicates that even the conservative E-fields from these innermost windings will be greatly altered or reduced if sufficiently long RF shields, shim coils, conductive coolant tubing, or other conductors exist between the gradient coils and the sample. Thus the conservative E-fields presented in Figs. 4 and 5 can be considered realistic only for a worst-case scenario in which there are no additional conductors between the innermost gradient windings and the subject.

Calculated E-Fields and PNS

There are many practical considerations involved with, and common-sense arguments against the proposition that conservative E-fields may play a major role in PNS for MRI. First, in the presence of a sufficiently long RF shield between the gradient coils and the subject, conservative E-fields from the gradient coil should be well shielded from the imaging region. In the case in which no sufficiently large conductors exist between the gradient windings and the subject, the conservative E-fields from the innermost windings would be expected to be much stronger than those from windings further outside (due to shielding effects of the innermost windings), and no observations of PNS being most easily induced from the innermost windings have been made. Due to the nature of the conservative E-fields as discussed above (or sometimes argued by considering the capacitance between the coil and the subject), they will induce no electrical currents of significant magnitude or duration within the subject. Furthermore, while human perception of conservative E-fields at power frequencies (50–60 Hz)—even to the point of being intolerable—was previously reported (23), it was attributed to the induced motion of hair or clothing. This makes it difficult to explain the symptom of involuntary muscle twitches often experienced in MRI as being produced by conservative E-fields.

Previous numerical calculations that examined only the magnetically-induced E-fields within the body often showed no real tendency for E-fields to be concentrated near the periphery of the body (13,17–19), although it is known from experiments that nerve stimulation generally occurs there. This is apparent in the lower portion of Fig. 3: the magnetically-induced E-fields just outside the body may be sizable, but within the body they are fairly well distributed throughout, and stronger E-fields are more apparent near boundaries of dissimilar conductivities deep within the body than near the surface of the body. This raises the question of whether the E-fields against the outside of the surface of the body should be considered as a source for PNS, since they generally (for either magnetically-induced or conservative E-fields, as in Figs. 3 and 4) are much larger than those just inside the surface. If it is possible that the fields just on the outer surface of the skin are important, then in cases with no significant shielding between the gradient coil and the subject, the conservative E-fields caused by ϕ_w on the innermost gradient windings could also be important, since they can produce very large E-fields at the outer surface of the skin. In calculations, the surface between the air and the conductive subject is theoretical and infinitesimally thin. In reality, it is somewhere just inside the body, and sensory nerve endings can be

within tens of microns from the dry stratum corneum and external air, depending on the location in the body. However, tens of microns may still be very large in terms of the thickness required for accumulation of a layer of charges to shield tissues from external fields. PNS in MRI also occurs in motor neurons toward the periphery of the body, which are generally farther still from the boundary with the dry stratum corneum.

It was previously proposed that the brief “flush” of charges toward the surface of the body resulting in partial shielding of the magnetically-induced E-fields may be responsible for PNS (24). If this is the case, perhaps the conservative E-fields caused by ϕ_w on the innermost windings should be reconsidered in the absence of significant shielding between the gradient coil and the subject, since these fields can potentially produce a larger flush of current resulting in greater charge accumulation at the surface. Also, some works have proposed spatial gradients in the E-field (rather than E-field or current magnitudes) as being the source of PNS (13). The single largest E-field gradient in the body would be that in skin adjacent to air, across the accumulated charges. The question again becomes one of how thick this boundary is in reality, and where the nerves are with respect to it.

A possible contribution of the magnetically-induced or conservative E-fields against the outer surface of the body in numerical calculations may also help to explain the lack of correlation between results of PNS experiments and existing theories related to the vector potential (9).

While it is generally held that conservative and magnetically-induced E-fields against the outer surface of the body, regardless of how large they are, are incapable of inducing PNS (except by motion of hair or clothing in some cases), the experiments that support this notion were generally conducted at a much lower frequency than that used for gradient coils in MRI. Because the sensitivity of nerves to applied E-fields is very much a function of the waveform of the applied fields (3), a reexamination of this with experiments using MRI-specific hardware and waveforms may be warranted.

ACKNOWLEDGMENT

B.A.C. currently holds the Canada Research Chair in Medical Physics at the University of Western Ontario.

REFERENCES

1. Cohen MS, Weisskoff RM, Rzedzian RR, Kantor HL. Sensory stimulation by time-varying magnetic fields. *Magn Reson Med* 1990;14:409–414.
2. Budinger TF, Fischer H, Hentschel D, Reinfelder H-E, Schmitt F. Physiological effects of fast oscillating magnetic field gradients. *J Comput Assist Tomogr* 1991;15:909–914.
3. Harvey PR, Mansfield P. Avoiding peripheral nerve stimulation: gradient waveform criteria for optimum resolution in echo planar imaging. *Magn Reson Med* 1994;32:236–241.
4. Irnich W, Schmitt F. Magnetostimulation in MRI. *Magn Reson Med* 1995;33:619–623.
5. Schaefer DJ, Bourland JD, Nyenhuis JA. Review of patient safety in time-varying gradient fields. *J Magn Reson Imaging* 2000;12:20–29.
6. King KF, Schaeffer DJ. Spiral scan peripheral nerve stimulation. *J Magn Reson Imaging* 2000;12:164–170.

7. Hoffman A, Faber SC, Werhan KJ, Jager L, Reiser M. Electromyography in MRI—first recordings of electrical nerve activation caused by fast magnetic field gradients. *Magn Reson Med* 2000;43:534–539.
8. Chronik BA, Rutt BK. A comparison between human magnetostimulation thresholds in whole-body and head/neck gradient coils. *Magn Reson Med* 2001;6:386–394.
9. Chronik BA, Ramachandran M. Simple anatomical measurements do not correlate significantly to individual peripheral nerve stimulation thresholds as measured in MRI gradient coils. *J Magn Reson Imaging* 2003;17:716–721.
10. Bencsik M, Bowtell R, Bowley RM. Electric fields induced in a spherical volume conductor by temporally varying magnetic field gradients. *Phys Med Biol* 2002;47:557–576.
11. Brand M, Heid O. Induction of electric fields due to gradient switching: a numerical approach. *Magn Reson Med* 2002;48:731–734.
12. Zhao H, Crozier S, Liu F. Finite difference time domain (FDTD) method for modeling the effect of switched gradients on the human body in MRI. *Magn Reson Med* 2002;48:1037–1042.
13. Liu F, Zhao W, Crozier S. On the induced electric field gradients in the human body for magnetic stimulation by gradient coils in MRI. *IEEE Trans Biomed Eng* 2003;50:804–811.
14. Bencsik M, Bowtell R, Bowley RM. Using the vector potential in evaluating the likelihood of peripheral nerve stimulation due to switched magnetic field gradients. *Magn Reson Med* 2003;50:405–410.
15. McKinnon G. A quasi-static FDTD approximation reduces computation time. In: Proceedings of the 11th Annual Meeting of ISMRM, Toronto, Canada, 2003. p 1438.
16. Collins CM, Chronik BA. Modeling human tissues in pulsed gradient fields. In: Proceedings of the 11th Annual Meeting of ISMRM, Toronto, Canada, 2003. p 2440.
17. McKinnon G. Simplifying gradient coil modeling in FDTD calculations. In: Proceedings of the 11th Annual Meeting of ISMRM, Toronto, Canada, 2003. p 2437.
18. Liu F, Xia L, Crozier S. Influence of magnetically-induced E-fields on cardiac electric activity during MRI: a modeling study. *Magn Reson Med* 2003;50:1180–1188.
19. Collins CM, Chronik BA, Smith MB. Significance of applied driving voltage in calculations of electrical fields in a loaded gradient coil. In: Proceedings of the 12th Annual Meeting of ISMRM, Kyoto, Japan, 2004. p 661.
20. Bowtell R, Bencsik M, Bowley R. Reducing peripheral nerve stimulation due to switched transverse field gradients using additional concomitant field coil. In: Proceedings of the 11th Annual Meeting of ISMRM, Toronto, Canada, 2003. p 2424.
21. Collins CM, Smith MB. Calculations of B_1 distribution, SNR, and SAR for a surface coil against an anatomically-accurate human body model. *Magn Reson Med* 2001;45:692–699.
22. Chronik BA, Rutt BK. Constrained length minimum inductance gradient coil design. *Magn Reson Med* 1998;39:270–278.
23. Clairmont BA, Johnson GB, Zafanella LE, Zelingher S. The effect of HVAC-HVDC line separation in a hybrid corridor. *IEEE Trans Power Deliv* 1989;4:1338–1350.
24. Forbes LK, Crozier S. On a possible mechanism for peripheral nerve stimulation during magnetic resonance imaging scans. *Phys Med Biol* 2001;46:591–608.